ISSN 2706-655X Vol.3, Issue 10: 1-13, DOI: 10.25236/IJFET.2021.031001

Improved Adaptive Butterfly Subdivision Algorithm and Its Application in 3D Geological Modeling

Jiajing Li[a*], Zhe Liu[b], Wei Wang[c]

School of Petroleum Engineering, Guangdong University of Petrochemical Technology, Maoming 525000, Guangdong, China
[a] lijiajing@gdupt.edu.cn, [b] liuzhe@gdupt.edu.cn, [c] 381583142@qq.com
**Corresponding author*

Abstract: *It is of great significance in the fields of 3D modeling, geological engineering and oil and gas storage. This paper mainly studies the improved adaptive butterfly subdivision algorithm and its application in 3D geological modeling. After the geological body section is created, the surface model can be constructed by connecting the sampling points on the contour line of adjacent sections with triangular patches according to the improved adaptive butterfly subdivision algorithm, and then the construction of the geological body model is realized by connecting the strata blocks with the same attributes on the adjacent sections. In this paper, the contour algorithm is used to generate the volume element surface. In this paper, the regular grid interpolation data is generated by butterfly subdivision algorithm using borehole data with multi-layer geological information. After all the simplexes in a 3D geological modeling area are generated, the complex body or complex to which the simple body belongs and the complex body to which the complex body belongs can be assigned. So far, the geological body simulation of 3D modeling area has been completed. Experimental data show that the total execution time of the algorithm is less than 20s. The results show that the improved butterfly subdivision algorithm can improve the accuracy and accuracy of the model.*

Keywords: *Improved Butterfly Algorithm, 3d Geological Modeling, Adaptive Subdivision, Data Model*

1. Introduction

With the increasing development and progress of scientific and technological civilization, optimization issues have become the focus of more and more attention. People living in different fields are constantly looking for ways to get the most benefits at the minimum cost. Furthermore, optimization methods have been gradually applied to various fields of social life. There is no effective connection between coal mining data, geological outcrops, well logging data, and seismic data, and cannot reflect the coal seams, strata and development characteristics three-dimensionally. Therefore, how to build a three-dimensional geological model that reflects the spatial distribution of coal seams, stratigraphic information and development characteristics is of great significance for rationally arranging well positions, optimizing well types, and improving oil recovery.

In daily life and production, to study collision detection, robot path planning and adjustment, tactile perception, it is often necessary to study the shortest distance between objects. For example, if the shortest distance between objects is zero, it means that objects will collide, then some measures should be taken to adjust the path. This paper starts from the whole process of 3D geological modeling, grasps the data unity and error analysis in different key technical links in the modeling process, uses the improved adaptive butterfly subdivision algorithm to improve the accuracy of 3D geological model, summarizes the research ideas and implementation methods of integrated high-precision 3D geological modeling, and provides scientific basis for the in-depth exploration and development of mature oilfield.

The improved butterfly algorithm is widely used in 3D geological modeling. Jiateng G believes that the three-dimensional geological model is an important expression of regional geological survey results. However, the process of constructing a 3D geological model from two-dimensional (2D) geological elements is still difficult and not necessarily reliable. He proposed a method to migrate from 2D elements to 3D models. First, he used hermite radial basis function (HRBF) to construct a geological interface with the purpose of interpolating boundary and attitude data. Then, he used the Boolean method between the HRBF surface and the matrix to extract the underground geological body from the spatial map area. Finally, he constructed the top surface of the geological body by coupling the

ISSN 2706-655X Vol.3, Issue 10: 1-13, DOI: 10.25236/IJFET.2021.031001

geological boundary with the digital elevation model. The factors considered in his research are not comprehensive [1]. Goncalves I G believes that implicit modeling has been popular over the past decade due to its advantages in speed and replicability. The potential field method includes interpolation scalar function based on punctuation data and structure direction, which indicates which side of geological boundary a given point belongs to. From the perspective of machine learning, he proposed the solution of vector potential field, recast the problem into multi class classification, thus alleviating some assumptions of the original method. He explained the potential associated with each geological category in the framework of the constituent data. He uses maximum likelihood training model to avoid variance graph modeling, and introduces uncertainty measurement. He applied the method to the modeling of the sample data set provided with the move software. His research lacks necessary experimental data [2]. Liu H believes that spatial interpolation is a main research method of 3D geological modeling, which has an important influence on the accuracy of 3D geological structure models. He introduced the concept of "correlation distance" to analyze the correlation between geological borehole elevation values and calculate the relative distance of each stratum elevation. He analyzed the distance-attenuation relationship in the interpolation neighborhood to correct the weight power value. He chooses sampling points to verify the calculation. His research is not very innovative [3]. Woloszyn I believes that the management of natural resources must follow the principle of sustainable development. He created a three-dimensional cross-border geological model. Taking into account the lithological changes and major structural structures, he combined part of the detailed stratigraphy of the Neogene sequence into five stratigraphic units. In addition, his model will serve as the basis for building a 3D cross-border groundwater model to study groundwater flow and migration in Miocene and Quaternary aquifer systems. Large amount of data and compatibility with other software are beneficial to the application of 3D geographic modeling software paradigmgocad. His research is not accurate [4].

This article mainly studies the improved adaptive butterfly subdivision algorithm and its application in 3D geological modeling. The original adjustment operator is changed to a shared adjustment operator with information sharing function to speed up the convergence speed of the algorithm; adopts greed the selection strategy replaces the elite retention strategy in the standard MBO, reducing one sorting operation and improving computational efficiency. This paper uses the improved adaptive butterfly subdivision algorithm to realize the dynamic model of 3D geological modeling. At the same time, it can provide the functions of graph visualization, square calculation, and automatic drawing of section maps, which provides new ideas for 3D geological modeling. It provides a route for the realization of 3D geological modeling in the BIM field.

2. Improved Adaptive Butterfly Subdivision Algorithm and 3D Geological Modeling

2.1 Improved Adaptive Butterfly Subdivision Algorithm

Because the sine and cosine are nonlinear, the linearity of Moir ésignal is also changed in real time, and the sampling sensitivity is not consistent in different phases. In particular, the voltage change rate near the peak value is very small, so it needs to detect a large angular displacement to cause a small voltage change, so it will produce a certain subdivision error. In the process of high multiple subdivision, the moire signal can not be quantized directly. In order to avoid the subdivision error caused by signal nonlinearity, the industry often uses the method of constructor for amplitude segmentation and subdivision [5].

The expression of the approximate triangular wave function is as follows:

$$u = |u_1| - |u_2| = |\sin\theta| - |\cos\theta| \tag{1}$$

In the case of considering only the DC drift, constant amplitude deviation and non-quadrature deviation of the signal, the mathematical model of the two output signals of the reading head is established:

$$\begin{cases} y_1 = A_1 + B_1 \cdot \sin\theta \\ y_2 = A_2 + B_2 \cdot \cos(\theta + \phi) \end{cases} \tag{2}$$

The formula for calculating the DC error of the signal is as follows:

ISSN 2706-655X Vol.3, Issue 10: 1-13, DOI: 10.25236/IJFET.2021.031001

$$\begin{cases} f(i-1) < f(i) > f(i+1) \\ DC = \dfrac{|f_{\max}| - |f_{\min}|}{2} \end{cases} \tag{3}$$

The loss function in SVM is represented by a hinge function:

$$L(f(w, x_i), y_i) = \max(0, 1 - y_i f(w, x_i)) \tag{4}$$

The loss function of RLS is expressed as:

$$L(f(w, x_i), y_i) = (y_i - f(w, x_i))^2 \tag{5}$$

For the function $f(x_i)$, the linear description is:

$$f(x_i) = < w, x_i > + b \tag{6}$$

Assuming the mapping function is $\varphi(x)$, then w becomes:

$$w = \sum_i \alpha_i \varphi(x) \tag{7}$$

Suppose the matrix composed of the results of the kernel function of the product between different samples is:

$$K_{ij} = k(x_i, x_j) \tag{8}$$

The final regression function is:

$$f(x_i) = \sum_{i=1}^{n} \alpha_i \kappa(x_i, x_j) \tag{9}$$

The circulant matrix has a very important property:

$$X = F^H diag(\hat{x}) F \tag{10}$$

In the formula, $\hat{x}$ represents the Fourier transform of x, and F is the discrete Fourier transform matrix.

If x is a circulant matrix, we can get:

$$w = F diag\left(\frac{\hat{x}}{\hat{x}^* \Theta \hat{x} + \lambda} \right) F^H y \tag{11}$$

The equivalent expression of the above formula in the frequency domain is:

$$\hat{w} = \frac{\hat{x}^* \Theta \hat{y}}{\hat{x}^* \Theta \hat{x} + \lambda} \tag{12}$$

The formula of the cross migration operator can be expressed as:

$$x_{i,k}^{t+1} = \begin{cases} c * x_{r_1,k}^t + (1-c) * x_{r_1,q}^t, r \le p \\ c * x_{r_2,k}^t + (1-c) * x_{r_2,q}^t, r > p \end{cases} \tag{13}$$

The greedy selection strategy formula is expressed as:

$$x_{i,new}^{t+1} = \begin{cases} x_i^{t+1}, f(x_i^{t+1}) < f(x_i^t) \\ x_i^t, otherwise \end{cases} \tag{14}$$

Among them, $x_{i,new}^{t+1}$ is the next generation of newly generated butterfly individuals, $f(x_i^{t+1})$

ISSN 2706-655X Vol.3, Issue 10: 1-13, DOI: 10.25236/IJFET.2021.031001

and $f(x_i^t)$ represent the fitness values of butterflies x_i^{t+1} and x_i^t, respectively.

The butterfly optimization algorithm realizes the update of candidate solutions through the exchange of information carried between the butterflies. The fitness ratio selection method is easy to cause premature convergence. This is because individuals with high fitness have a greater chance of entering the next generation, while the remaining individuals have a small chance, resulting in a narrowing of the optimization range and finally converging to the local optimum. The initial stage is different from the later stage. At this time, the better individuals in the group almost maintain a stable state, and it is not certain that the optimal solution of the current state is the all optimal solution to the problem, which increases the risk of the algorithm falling into the local optimal solution [6-7]. The overall flow of the MBO algorithm is shown in Figure 1. For the optimization problems of complex systems, especially the problems that are difficult to solve with traditional search algorithms, evolutionary algorithms have unique advantages. The traditional butterfly subdivision algorithm has better robustness for solving optimization problems with fewer optimization parameters and linearization optimization, but for problems with more complex objective functions and more optimization variables, traditional algorithms are not easy to search for the global optimal solution. The convergence speed is slow and the stability is poor [8]. The improved butterfly segmentation algorithm not only increases the reproduction opportunities of excellent individuals, but also avoids the over-reproduction of some excellent individuals with higher fitness, resulting in the decrease of group diversity and the premature convergence of solutions. Although the fitness value of an individual is related to whether the individual satisfies the constraints, the individual with a higher fitness may still be an infeasible solution, which will eventually lead to an infeasible solution. Therefore, before the replacement, a comprehensive comparison of the newly generated individual and the fitness of the individual in the original population and the feasibility of the solution [9].

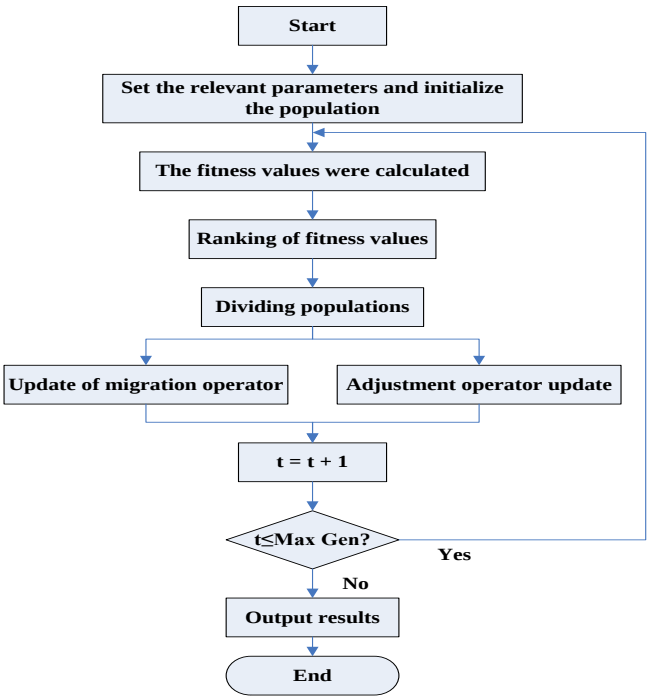

Figure 1: The overall flow of the MBO algorithm

2.2 Three-Dimensional Geological Modeling

The basic geometric elements of the model include points and lines. The points on the object boundary are linked by line segments, called curves or polygons, as the skeleton of 3D modeling. However, this method cannot process the internal details of the entity [10]. The process of modeling often involves the identification, interpretation, description, positioning and representation of complex strata, ore bodies and geological structures, which is also the difficulty of 3D geological modeling technology. The underground geology itself has the characteristics of complexity, gradual change and mutation, such as strata folds, faults, joint fissures and some other random underground karst rocks, with various shapes [11].

ISSN 2706-655X Vol.3, Issue 10: 1-13, DOI: 10.25236/IJFET.2021.031001

The three-dimensional frame grid is divided into three layers: top, middle and bottom. The topological relationship between each layer is the same. First of all, the middle grid is generated by corner mesh generation. On the middle grid node, all grid nodes are inserted into grid column according to the trend of fault column, and the top and bottom grid of frame grid are formed through the key points of grid column. The role of the frame grid model is to roughly define the spatial structure of the geological structure model, and the final structure model is realized by inserting strata [12-13].

The solid model overcomes this shortcoming of the surface model, can more completely and comprehensively describe the spatial structure and internal characteristics of geological objects, can better support geological analysis, reserve estimation, and facilitate the staff to understand the geological situation [14]. But relatively speaking, the entity model is more complicated than the surface model in terms of data structure and data organization. The modeling process needs to deal with a lot of information, and the modeling efficiency is low. The variability of geological conditions, the complexity of information, and the difficulty of global prediction have resulted in the characteristics of multi-source and multi-dimensional geological data. These characteristics determine the richness of data sources, and also bring about the huge amount of data, the variety of types, and the complexity of the structure [15].

With the continuous development of information technology of geological and mineral work, the corresponding amount of data is also increasing, the data types tend to be more diversified and the structure is more complex. As the basic data of the whole system, the quality of plane geological map directly affects the accuracy and efficiency of modeling, and its structure determines the way of data management. Since the starting and ending positions of the sampling section are not completely coincident with the borehole inclinometer point, the spatial position of the sampling section should be consistent with the borehole trajectory. By judging the position of the starting and ending points of the sampling section, according to the principle of similar triangle, the interpolation calculation can be carried out, and the interpolation coordinates of the sampling section can be finally obtained [16-17].

2.3 Model Visualization

Visualization technology can use computer image processing technology to express various data involved in the process of scientific research in the form of graphic images, allowing people to directly manipulate three-dimensional spatial data, opening up a scientific research space for creative thinking. Digital visualization technology supports the establishment of the entire 3D model, and 3D modeling lays the foundation for the visualization of the spatial geometry of complex geological bodies. In order to better display the three-dimensional model and understand the spatial relationship between geometric bodies, coordinate axes can be added to the scene. At the same time, the coordinate axis can help the observer to more accurately understand the posture of the 3D object in space, and can also analyze and help solve the problems of the viewport, the position and angle of the camera and the light [18].

Unfortunately, WPF does not provide a class for drawing straight lines in three-dimensional space. It is more troublesome to render long and narrow triangles to approximate straight line segments in space. A triangle in space has two front and rear faces. The face with the vertices arranged counterclockwise is the front of the triangle, and the clockwise is the back. A point in the space contains multiple attributes, including basic attributes such as the position of the point, color, and other attributes such as the index connected to the viewport position and selected editing. The accuracy of the 3D geological model is affected by the original drilling data and spatial interpolation. In order to improve the accuracy of the model, not only the actual engineering experience and multi-source geological data are effectively combined, but also the unknown area of space can be fitted by reasonable interpolation methods [19].

The essence of spatial data interpolation is to fit unknown data through known data, which is an important technique for constructing three-dimensional stratigraphic models. These values are connected by a series of points on the line to form airtight triangles inside and outside. These triangles appear to intersect and overlap in the plane, but in three-dimensional space, there is no overlap between any triangles. In the 3D block stratum structure model, each stratum block can be regarded as an independent geological block with its own geological attributes and envelope surface. Therefore, any complex 3D geological model can be used as a simple geological block. The geological block units are independent of each other and do not intersect each other [20-21].

ISSN 2706-655X Vol.3, Issue 10: 1-13, DOI: 10.25236/IJFET.2021.031001

3. Three-Dimensional Geological Modeling Simulation Experiment

3.1 Model Attribute Set

When creating non-geometric attributes of a 3D geological model, it needs to be created in the form of an attribute set, which is a container for storing attributes. The attribute set must contain at least one attribute. When it contains multiple attributes, the content and meaning of the attribute are characterized by its name, regardless of its order in the attribute set [22]. The attribute set created in this article is shown in Table 1.

Table 1: Attribute set

Property name	Property type	Data type
Formation Type	Single Value	string
Particle Diameter	Single Value	double
Weathering Degree	Enumerated Value	string
Orientation	Single Value	string

3.2 Model Establishment

After the geological body section is created, the surface model can be constructed by connecting the sampling points on the contour line of adjacent sections with triangular patches according to the improved adaptive butterfly subdivision algorithm, and then the construction of the geological body model is realized by connecting the strata blocks with the same attributes on the adjacent sections.

(1) The method of defining the boundary of volume element and mid section of volume element is to determine a simple geological body to be simulated on the section, and then specify the volume element identification, the simple body identification, the section identification and various attribute values, and then draw the boundary of the mid section of the volume element with the mouse. The topological relationship between adjacent voxels on the profile can be automatically generated by the program [23].

(2) After the boundary of the middle section of the voxel is defined, the user can specify the space distance between the front and back sections of the voxel to form the extended section. In this case, if the adjacent voxels have different expansion patterns on the common spreading section, they must be adjusted so that their boundary morphology on the common spreading section is the same.

(3) Generation of voxel surface: voxel surface is a part of the peripheral interface of voxel. It is formed by connecting the arc contour lines of the voxel and the points on it. The connection modes are constrained and unconstrained, which are generated by contour algorithm [24].

When the voxels of adjacent simple bodies are generated, because the topology data structure is adopted, the adjacent boundary lines on the same section can be no longer drawn, thereby avoiding the disadvantage of drawing the same section repeatedly without a topological data structure. After all the simple bodies in a 3D geological modeling area are generated, the complex body or complex to which the simple body belongs and the complex to which the complex body belongs can be specified. So far, the geological body simulation of the 3D modeling area has been completed [25].

3.3 Model Optimization

Discretely distributed drilling data is not only an important data support for constructing raster data models, three-dimensional geological models, but also three-dimensional drilling models can describe complex geological attribute information and internal geological structures. There are certain errors in the way of constructing a three-dimensional geological model to simulate the real stratum. Geologists can use the geological profile map provided by the survey institute to add control point constraints in the 3D geological modeling process to optimize the interpolation results and achieve the goal of being closer to the actual geology [26].

3.4 Data Analysis

In addition to the characteristics of general data in 3D geological attribute data, each data is also related to its location. To fully understand these data and prepare for the selection of appropriate

ISSN 2706-655X Vol.3, Issue 10: 1-13, DOI: 10.25236/IJFET.2021.031001

parameters and methods, it is necessary to use some exploratory spatial data analysis tools, including histograms, scatter plots, variograms, etc. Through these exploratory spatial data analysis tools, you can determine data attributes, detect data distribution, global and local outliers, study spatial autocorrelation, and understand the correlation between multiple data sets [27-28].

4. Model Simulation Analysis

4.1 Algorithm Accuracy Analysis

The analysis of structural characteristics of variogram quantitatively represents the structural distribution information of sample data and describes the information characteristics of regionalized variables. This part includes the calculation and fitting of variogram. The calculation of variogram is based on the data sample information to construct the discrete measured value of variogram, and the fitting of variogram is to fit an optimal curve by discrete points. The model parameters are shown in Table 2. Different variogram fitting results are shown in Figure 2. It can be seen that the curve fitting structure reflects the characteristics of regionalized variables in different directions. When the distance between the curve is small, the fitting effect is more consistent with the experimental variogram value, which indicates that the attribute value has certain spatial autocorrelation in all directions, which has structural characteristics; the experimental variogram has obvious variation in three directions, but the trend is different, it is anisotropic. The results show that the traditional hierarchical sliding mode control algorithm and the adaptive fuzzy layered sliding mode control algorithm converge to the expected value in 4S; the response speed of the adaptive fuzzy layered sliding mode algorithm is obviously faster than that of the traditional hierarchical sliding mode control algorithm; the maximum deviation of the adaptive fuzzy layered sliding mode algorithm relative to the expected value is obviously smaller than that of the traditional hierarchical sliding mode algorithm.

Table 2: Model parameters

	Abutment value	Variation	Nugget value	Model
First axis	2.8	70	0.7	Spherical model
Second axis	4.8	65	2.1	Spherical model
Third axis	5.4	64	1.9	Index model

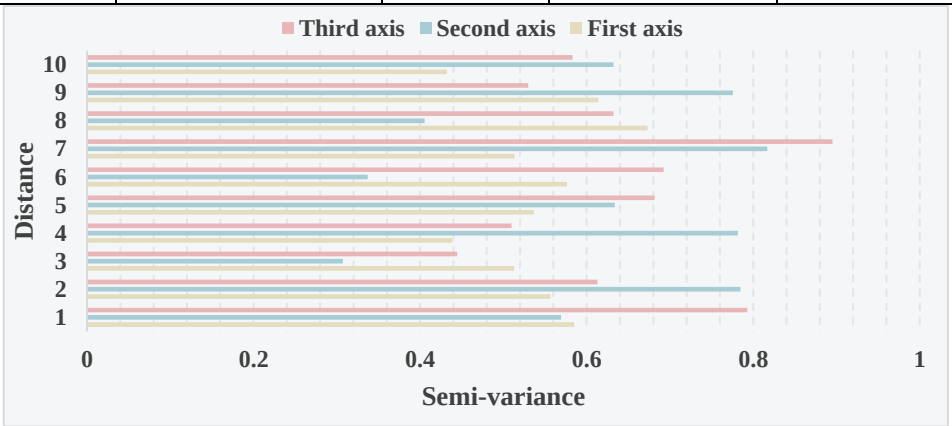

Figure 2: Fitting effects of different variograms

The fitting results of the three methods are shown in Table 3. From the data in the table, it can be seen that the spherical model has a certain ability of crosswell prediction. Most of the predicted data are similar to the actual sampling data, but there is a large data deviation. For example, the actual sampling value is 2.54, while the estimated value is 5.32. The cross well prediction ability of the local weighted method is poor, and the deviation between the estimated value and the actual sample value is large. The result of cubic polynomial fitting method is the best. In all experimental data, the estimated value is the closest to the actual sample value, and the prediction ability is the best. By observing the estimated values of the three methods and the actual sample values, it can be found that the estimation results of spherical model and cubic polynomial are similar, and they are very close to the sample values; while the local weighted fitting method can obtain more realistic results in most data. However, in the last two rows of experimental data in the table, there are abnormal estimation results, which is caused by the discontinuity of semi variogram. Comparing the visualization effect of the original plane geological

ISSN 2706-655X Vol.3, Issue 10: 1-13, DOI: 10.25236/IJFET.2021.031001

map and the geological body model, it can be seen that the geological model established in this paper can basically reflect the geological conditions of the shallow strata in the study area, which proves that the method of 3D geological modeling based on the plane geological map proposed in this paper is effective and feasible.

Table 3: Fitting estimation results of the three methods

Numbering	Sample value	Spherical fit estimate	Locally weighted fit estimate	Estimated value of cubic polynomial fit
1	1.65	1.69	1.71	1.69
2	1.81	1.71	1.72	1.72
3	5.53	5.65	5.65	5.64
4	0.62	0.60	0.59	0.61
5	2.72	2.76	2.94	2.75
6	2.63	2.82	-9.12	2.86
7	2.45	2.81	-8.21	2.82

According to the different parameters of the sampled values, we compared the three methods of in-well estimation experiments, as shown in Figure 3. It can be seen that the mean and variance of spherical model and cubic polynomial estimation results are approximate to the actual sample value, and the average error is small; while the mean value of local weighted method is slightly worse, and the estimation variance is larger and the average error is larger due to the interference of abnormal estimation results. Based on the above experimental results, the spherical model and cubic polynomial can well describe the spatial variability of attributes, with high interpolation accuracy, stable algorithm, and high reliability of estimation results; on the whole, the local weighted fitting method can obtain satisfactory estimation results, but its semi variogram model is piecewise function. As a result, there will be abnormal estimation results in a specific location, which reduces the accuracy of the algorithm, and the credibility is lower than the former two methods.

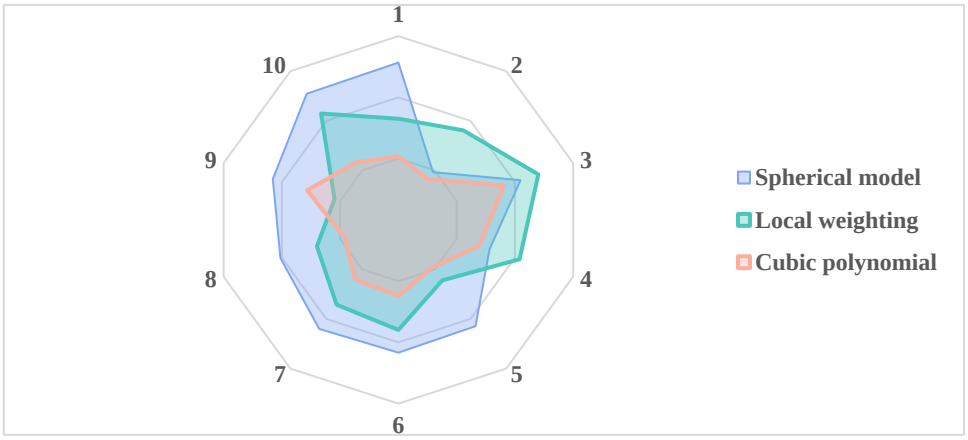

Figure 3: In-well estimation comparison of the three methods

4.2 Influence of Improved Butterfly Subdivision Algorithm on Model

The grid statistics before and after interpolation and subdivision are shown in Figure 4. From the data in the figure, it can be seen that the loop and full correlation algorithm based on triangular mesh subdivision have the same number of nodes, edges and mesh faces after each subdivision. For the Catmull-Clark subdivision algorithm with quadrilateral mesh, the number of mesh faces is basically the same, but the number of nodes and edges are obviously more than the other two subdivision methods. With the increase of the number of subdivisions, each error curve approaches a certain constant value. This shows that no matter it is interpolation, Catmull-Clark or Loop subdivision methods, they are all convergent. And after the first two to three subdivisions, the error no longer changes greatly, indicating that the subdivision surface has approached the limit surface. Different from the interpolation subdivision method, the error of Catmull-Clark and Loop subdivision surfaces tends to increase, while the interpolation surface will continuously reduce the error. The error of the initial grid is 0.8179, the interpolation subdivision reduces the error to 0.2848, while the Catmull-Clark subdivision makes the error rise to 1.011, and the Loop subdivision makes the error reach 1.15.

ISSN 2706-655X Vol.3, Issue 10: 1-13, DOI: 10.25236/IJFET.2021.031001

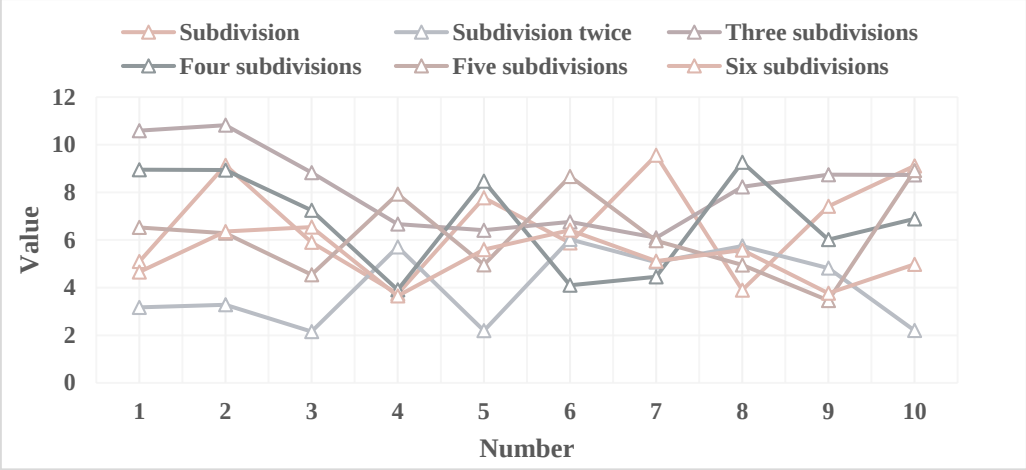

Figure 4: Grid statistics before and after interpolation and subdivision

The algorithm data statistics in this paper are shown in Figure 5. If the unknown point is affected by only one known point, the influence can be directly calculated by the weight function defined by distance, which can be linear or nonlinear, and sometimes the attribute of unknown point can be calculated by exponential method. However, in reality, unknown points are always affected or constrained by many known points, which requires comprehensive consideration of these known points. When iterating for 25 generations, the data of 50 repeated experiments is 31.548, the average value of 100 iterations is 31.472, the average value of 150 iterations is 31.536, and the average value of 200 iterations is 31.526. Therefore, we can see that our optimal value is about 31.5 when iterating 25 generations. When iterating 50 generations, the data of 50 iterations is 29.634, the average value of 100 iterations is 29.722, the average value of 150 iterations is 29.952, and the average value of 200 iterations is 30.073. Therefore, we can see that our optimal value is about 29.9 in the 50 generations of iterations. According to the data in the figure, it can be concluded that the optimal value is 31.5 in 25 generations, 29.9 in 50 iterations, 28.9 in 100 generations, and 26.5 in 200 generations. We can clearly see that our optimal value is reduced by about 5 values.

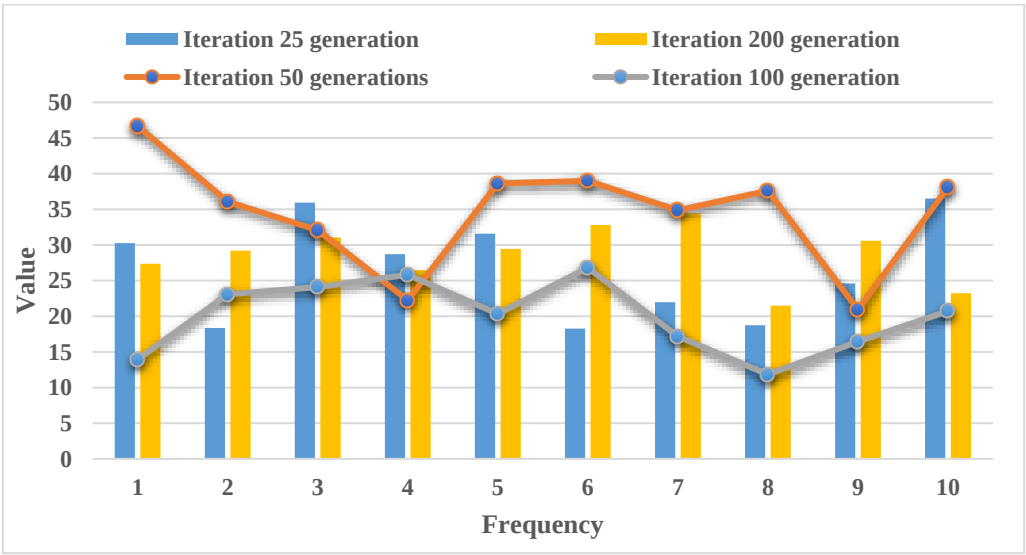

Figure 5: The algorithm data statistics of this article

The comparison of clustering results of opmbo algorithm, MBO algorithm and gcmbo algorithm is shown in Table 4. The mean and STD values of 10 datasets obtained by opmbo algorithm are optimal. The mean of opmbo algorithm is about 5% - 6% higher than gcmbo algorithm, and about 4% - 7% higher on heart, liverdisorders and statlog datasets. However, on these three datasets, the difference of STD value between opmbo algorithm, MBO algorithm and gcmbo algorithm is about 1%. Although the opmbo algorithm achieves the mean and STD optimal values on the other seven datasets, the results of opmbo algorithm are very close to MBO algorithm and gcmbo algorithm. In a word, opmbo algorithm can achieve satisfactory results on these 10 datasets.

ISSN 2706-655X Vol.3, Issue 10: 1-13, DOI: 10.25236/IJFET.2021.031001

Table 4: Comparison of clustering results

Data set	Value	MBO	GCMBO	OPMBO
Mydata	Mean	1.8159	1.7644	1.5715
	Std	0.1740	0.1710	0.1382
Abalone	Mean	1.8487	1.8430	1.6846
	Std	0.1259	0.1135	0.0904
Balance Scale	Mean	2.3613	2.3647	2.3250
	Std	0.0237	0.0238	0.0147
Car	Mean	2.0465	2.0478	2.0125
	Std	0.0227	0.0214	0.0193

The accuracy comparison of KCF, SKCF, SMKCF, SMIKCF, SAMF algorithm in 50 test video sequences of Benchmark is shown in Figure 6. The SMKCF algorithm that extracts HOG+CN fusion features has higher success rate and accuracy than the SKCF algorithm that only extracts HOG features, the success rate is improved by 1.0%, and the accuracy is improved by 0.9%. The description ability of the HOG feature itself has been relatively strong, and the performance has been improved after adding the CN feature, but the improvement is not much. Compared with the SMKCF algorithm, the SMIKCF algorithm improved by using APCE for template update strategy has improved the success rate and accuracy, the success rate has increased by 3.8%, and the accuracy has increased by 2.9%. It shows that the template update strategy is very important, and a suitable template update strategy can improve the performance of the target tracking algorithm.

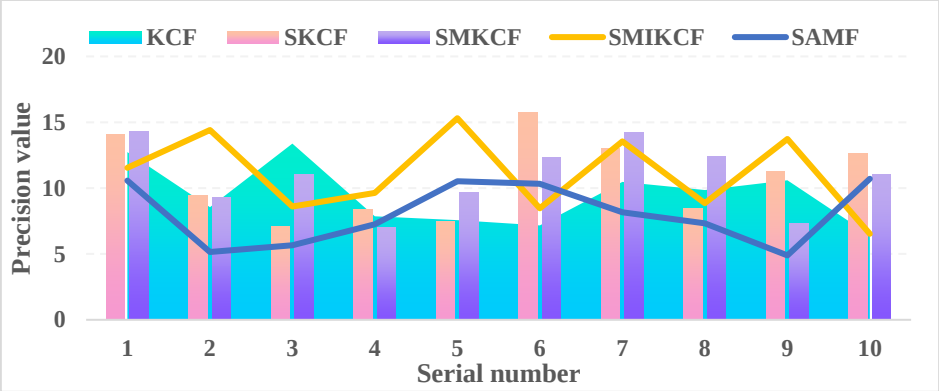

Figure 6: Accuracy comparison of different algorithms

4.3 Algorithm Accuracy Analysis

The effect of different interpolation methods on the geological model is shown in Figure 7. The algorithm based on feature polygons does not need to record any additional data, as long as you know the mesh data after subdivision, the difference is that the Kriging algorithm needs to record a known clone surface in the initial mesh data at the same time. It is the reverse segmentation of the data before the known segmentation, and it is not completely based on the known data after the segmentation. This algorithm is faster than the weighting algorithm and is more convenient to implement.

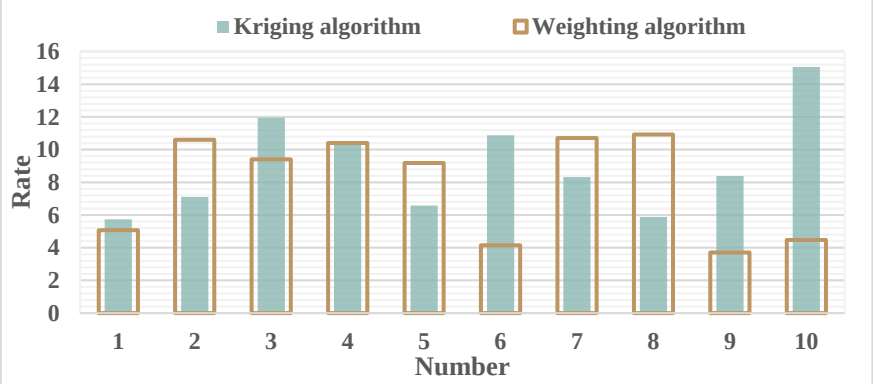

Figure 7: The effect of different interpolation methods on the geological model

ISSN 2706-655X Vol.3, Issue 10: 1-13, DOI: 10.25236/IJFET.2021.031001

The running results of the algorithm are shown in Table 5 and Figure 8. The cube subdivision scale used in this test is 50. The total execution time of the algorithm is less than 20s when tracking all stratigraphic blocks. It can be seen from the chart that the shape of the block is basically normal, and there is no breakage, hollowing out and breakage. However, all the blocks traced out contain some wrong blocks, which are usually very small. This may be because the subdivision scale of the model is not fine enough, which leads to the block chasing program failing to pass through some narrow space, so as to trace out the blocks with very small shape. In addition, the block chasing program automatically forms a stratigraphic block above the ground surface and below the upper surface of the work area, this block can be removed manually or programmatically.

Table 5: The running results of the 3D fuzzy block tracking algorithm

A	6.82	7.95	14.48	10.15	10.31	11.76	11.33	13.56	9.30	11.07
B	9.93	13.85	13.76	13.48	15.89	11.63	14.25	6.94	7.74	10.26
C	10.67	6.23	13.93	10.21	10.85	9.63	7.55	10.55	10.87	6.62

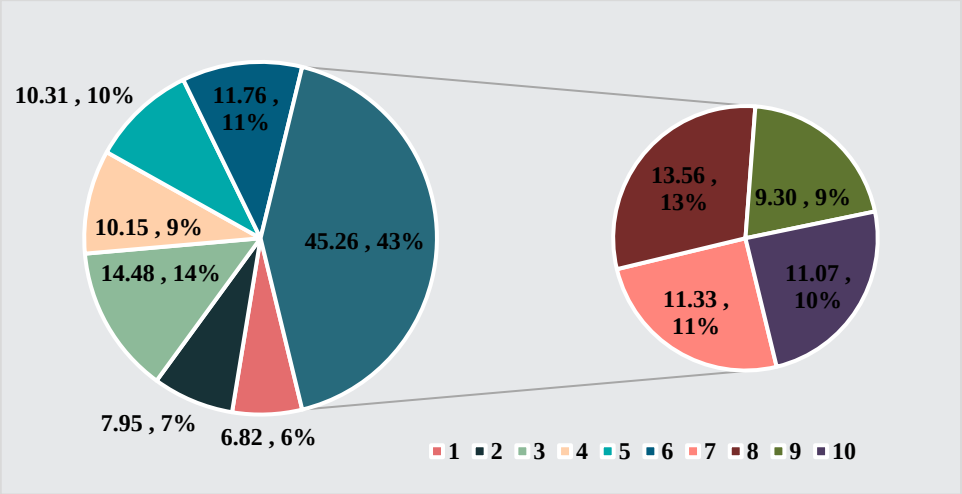

Figure 8: The running results of the 3D fuzzy block chasing algorithm

The determination of the length of the combined sample in the sample combination is a very important step in the modeling process of the deposit resource model. From the theory and practice, it is reasonable to take the average of the length of the original sample. The length of the combined sample is 1.15m, the average length of the original sample. The statistical characteristic values are shown in Table 6. It can be found that compared with the statistical parameters of the original sample, the average value and standard deviation of element grades are basically the same before and after the sample combination, which shows that the sample has a small change after the special high grade treatment and combination. The improved butterfly subdivision algorithm can accurately detect the harmonic components. Since the load current has a sudden change at the beginning, the detected harmonics still have more high-order harmonic components at the beginning. Using the Powergui module in MATLAB power system simulation to analyze the load current harmonics, it is found that the load current contains larger harmonic components such as the 1, 5, 7 and 11 orders, and the total harmonic distortion rate is 30.84%.

Table 6: Statistical feature values

Element	Minimum	Max	Average value	Standard deviation	Median	Number of samples
Cu	0.002%	3%	0.4973%	0.4486	0.3409%	23611
TFe	0.2453%	49.15%	21.6832%	6.4525	21.4995%	14106
SFe	0.0125%	46.77%	20.2894%	6.5756	19.9502%	12080

5. Conclusions

In this paper, the density of the data points is increased by inserting the points to be inserted, the neighborhood of each point and its weight coefficient are changed, and the final value of each point is determined by iterative calculation. This method can not only adjust the accuracy of the generated

ISSN 2706-655X Vol.3, Issue 10: 1-13, DOI: 10.25236/IJFET.2021.031001

surface by selecting the number of iterations, but also the geological surface can also be optimized by adjusting the number of points to be inserted and the topological relationship. In this paper, a real three-dimensional geological model of the mine is constructed based on the quasi-triangular prism model. Experiments show that this modeling method can quickly and accurately construct a three-dimensional model of complex geological bodies, reducing the workload of manual interactive modeling.

According to the trend and shape of each stratum, a closed surface which can contain the geological boundary and drilling points of the stratum is established in a certain elevation plane, and then the deformation of the curved surface is controlled according to the geological boundary and drilling points as control constraint points. The formation interface is formed when the deformed curved surface passes through the geological boundary and drilling point of this layer. The grid model does not depend on the distribution characteristics of the original sampling data, and can be well used in various data distribution situations. The equilateral triangle grid is one of the better mesh models, which has the advantages of GRID and TIN.

The solid model actually displays the two-dimensional geological information in the three-dimensional space, and can clearly and intuitively display the morphological characteristics and mutual relationships of various geological objects in the three-dimensional space. In this paper, by dividing different geomorphic type units, according to geomorphic features, combined with drilling data, design the bedrock depth estimation method for different geomorphic type units, and on this basis, complete the bedrock surface modeling constrained by geomorphic features.

Acknowledgements

This work was supported by The National Natural Science Foundation of China (41602154) and Projects of Talents Recruitment of GDUPT (2018rc01)

References

[1] Jiateng G , Lixin W , Wenhui Z , et al. Towards Automatic and Topologically Consistent 3D Regional Geological Modeling from Boundaries and Attitudes[J]. International Journal of Geo-Information, 2016, 5(2):1-17.

[2] Goncalves I G , Kumaira S , Guadagnin F . A machine learning approach to the potential-field method for implicit modeling of geological structures[J]. Computers & Geoences, 2017, 103(6):173-182.

[3] Liu H , Chen S , Hou M , et al. Improved inverse distance weighting method application considering spatial autocorrelation in 3D geological modeling[J]. Earth ence Informatics, 2020, 13(3):619-632.

[4] Woloszyn I , Merkel B , Stanek K . 3D geological modeling of the transboundary Berzdorf-Radomierzyce basin in Upper Lusatia (Germany/Poland)[J]. International Journal of Earth ences, 2017, 106(5):1651-1663.

[5] Hao M , Wang D , Deng C , et al. 3D geological modeling and visualization of above-ground and underground integration ——taking the Unicorn Island in Tianfu new area as an example[J]. Earth ence Informatics, 2019, 12(4):465-474.

[6] Martinez J L , Raiber M , Cendon D I . Using 3D geological modelling and geochemical mixing models to characterise alluvial aquifer recharge sources in the upper Condamine River catchment, Queensland, Australia[J]. ence of The Total Environment, 2017, 574(1):1-18.

[7] Maesano F E , D'Ambrogi C . Vel-IO 3D: A tool for 3D velocity model construction, optimization and time-depth conversion in 3D geological modeling workflow[J]. Computers & Geoences, 2017, 99(2):171-182.

[8] Mohamed, Hamdi, Mohamed, et al. 3D geological modeling for complex aquifer system conception and groundwater storage assessment: Case of Sisseb El Alem Nadhour Saouaf basin, northeastern Tunisia[J]. Journal of African Earth ences, 2018, 143(7):178-186.

[9] Milicich S D , Pearson-Grant S C , Alcaraz S , et al. 3D Geological modelling of the Taupo Volcanic Zone as a foundation for a geothermal reservoir model[J]. New Zealand journal of geology & geophysics, 2018, 61(1):79-95.

[10] Hofmayer F , Kirscher U , Sant K , et al. Three-dimensional geological modeling supports a revised Burdigalian chronostratigraphy in the North Alpine Foreland Basin[J]. International Journal of Earth ences, 2019, 108(8):2627-2651.

ISSN 2706-655X Vol.3, Issue 10: 1-13, DOI: 10.25236/IJFET.2021.031001

[11] Vilà, Miquel, Torrades P , Pi R , et al. The role of 3D modelling in the urban geological map of Catalonia[J]. Ztschrift der Deutschen Gesellschaft für Geowissenschaften, 2016, 167(4):389-403.
[12] Rautenberg S , Schmitz T , Sibul I , et al. Challenges and opportunities of geological 3D modelling – a case study for the northeastern part of Estonia[J]. Ztschrift Der Deutschen Gesellschaft Für Geowissenschaften, 2016, 167(4):353-361.
[13] Zhang Y , Zhong D , Wu B , et al. 3D Parametric Modeling of Complex Geological Structures for Geotechnical Engineering of Dam Foundation Based on T-Splines[J]. 2018, 33(7):545-570.
[14] Zhi-Ning L , Cheng-Yun S , Zhi-Yong L , et al. 3D modeling of geological anomalies based on segmentation of multiattribute fusion[J]. Applied Geophysics, 2016, 13(003):519-528.
[15] Cai B , Zhao J , Yu X . A methodology for 3D geological mapping and implementation[J]. Multimedia Tools and Applications, 2019, 78(20):28703-28713.
[16] Yang L , Hyde D , Grujic O , et al. Assessing and visualizing uncertainty of 3D geological surfaces using level sets with stochastic motion[J]. Computers & Geoences, 2019, 122(1):54-67.
[17] Elyasi A , Javadi M , Moradi T , et al. Numerical modeling of an umbrella arch as a pre-support system in difficult geological conditions: a case study[J]. Bulletin of engineering geology and the environment, 2016, 75(1):211-221.
[18] Xiong Z , Guo J , Xia Y , et al. A 3D Multi-scale geology modeling method for tunnel engineering risk assessment[J]. Tunnelling and Underground Space Technology, 2017, 73(3):71-81.
[19] Eldursi K , Branquet Y , Guillou-Frottier L , et al. Intrusion-Related Gold Deposits: new insights from gravity and hydrothermal integrated 3D modeling applied to the Tighza gold mineralization (Central Morocco)[J]. Journal of African Earth ences, 2018, 140(4):199-211.
[20] Yousefi M, Carranza E J M. Data-Driven Index Overlay and Boolean Logic Mineral Prospectivity Modeling in Greenfields Exploration [J]. Natural Resources Research, 2016, 25(1):3-18.
[21] Yucel M A, Turan R Y . Areal Change Detection and 3D Modeling of Mine Lakes Using High-Resolution Unmanned Aerial Vehicle Images[J]. Arabian Journal for ence & Engineering, 2016, 41(12):1-12.
[22] Ou C, Li C . 3D discrete network modeling of shale bedding fractures based on lithofacies characterization[J]. Petroleum Exploration and Development, 2017, 44(2):336-345.
[23] Codegone G , Rocca V , Verga F , et al. Subsidence Modeling Validation Through Back Analysis for an Italian Gas Storage Field[J]. Geotechnical and Geological Engineering, 2016, 34(6):1749-1763.
[24] Priyanka B N , Kumar M S M . Direct and inverse modeling of seawater intrusion: A perspective[J]. Journal of the Geological Society of India, 2017, 90(5):595-601.
[25] Vassallo R , Mishra M , Santarsiero G , et al. Modeling of Landslide–Tunnel Interaction: the Varco d'Izzo Case Study[J]. Geotechnical and Geological Engineering, 2019, 37(6):5507-5531.
[26] Saikia K . A proposed methodology of 3D geomodeling-while-geosteering for optimum horizontal well placement and enhanced geological risk management [J]. Indian Journal of Marine ences, 2018, 47(4):826-830.
[27] Jia Q , Che D , Li W . Effective coal seam surface modeling with an improved anisotropy-based, multiscale interpolation method [J]. Computers & Geosciences, 2018, 124(3):72-84.
[28] Xie J , Wang G , Sha Y , et al. GIS prospectivity mapping and 3D modeling validation for potential uranium deposit targets in Shangnan district, China[J]. Journal of African Earth Sciences, 2016, 128(4):161-175.